Continuous-Flow Chemical Synthesis for Sub-2 nm Ultra-Multielement Alloy Nanoparticles Consisting of Group IV to XV Elements

Hiroki Minamihara[1], Kohei Kusada[1,2]*, Tomokazu Yamamoto[3], Takaaki Toriyama[3], Yasukazu Murakami[3], Syo Matsumura[4], Loku S. R. Kumara[5], Osami Sakata[5], Shogo Kawaguchi[5], Yoshiki Kubota[6], Okkyun Seo[5], Satoshi Yasuno[5], Hiroshi Kitagawa[1]*

[1]Division of Chemistry, Graduate School of Science, Kyoto University, Kitashirakawa-Oiwakecho, Sakyo-ku, Kyoto 606-8502, Japan.

[2]The HAKUBI Center for Advanced Research, Kyoto University, Kitashirakawa-Oiwakecho, Sakyo-ku, Kyoto 606-8502, Japan.

[3]The Ultramicroscopy Research Center, Kyushu University, 744 Motooka, Nishi-ku, Fukuoka 819-0395, Japan.

[4]National Institute of Technology, Kurume College, 1-1-1 Komorino, Kurume-shi, Fukuoka 830-8555, Japan.

[5]Center for Synchrotron Radiation Research, Japan Synchrotron Radiation Research Institute (JASRI) SPring-8, 1-1-1 Kouto, Sayo-cho, Sayo-gun, Hyogo 679-5198, Japan.

[6]Department of Physics, Graduate School of Science, Osaka Metropolitan University, 1-1 Gakuen-cho, Naka-ku, Sakai, Osaka 599-8531, Japan.

ABSTRACT: Multielement alloy nanoparticles have attracted much attention due to their attractive catalytic properties derived from the multiple interactions of adjacent multielement atoms. However, mixing multiple elements in ultrasmall nanoparticles over a wide range of elements on the periodic table is still challenging because the elements have different properties and miscibility. Herein, we developed a benchtop 4-way flow reactor for chemical synthesis of ultra-multielement alloy (UMEA) nanoparticles composed of d-block and p-block elements. BiCoCuFeGaInIrNiPdPtRhRuSbSnTi 15-element alloy nanoparticles composed of group IV to XV elements were synthesized by sequential injection of metal precursors using the reactor. This methodology realized the formation of UMEA nanoparticles at low temperature (66 °C), resulting in a 1.9-nm ultrasmall average particle size. The UMEA nanoparticles have high durability and activity for electrochemical alcohol oxidation reactions and high tolerance to CO poisoning. These results suggest that the multiple interactions of UMEA efficiently promote the multistep alcohol oxidation reaction.

INTRODUCTION

Solid-solution alloy nanoparticles (NPs) show unique properties derived from the interaction between different elements, and many synthesis methods have been developed for a long period of time[1–6]. Recently, multielement-alloy (MEA) NPs, for example, high-entropy alloy (HEA) NPs consisting of 5 or more elements, have attracted much attention, especially for their captivating catalytic properties, which are completely different from those of conventional alloy catalysts[7,8]. This may be because every atom tends to have a different electronic structure due to various configurations of adjacent atoms[9]. However, the electronic state of atoms is altered based on the original electronic state of the elements. In order to achieve suitable local electronic states for catalytic reactions incorporating various intermediates, it would be suitable to mix elements with widely different properties from a wide range of the periodic table of the elements. Although many kinds of synthesis methodologies for MEA NPs have been rapidly developed in the last 5 years[10–12], mixing ultra-multiple elements, such as more than 10 elements, is still challenging due to the different properties and miscibility of each element. Additionally, although small particle sizes with high surface-to-volume ratios are advantageous for catalytic applications[13], high-temperature synthesis conditions that efficiently utilize high configurational entropy often result in relatively larger particle sizes (over 10 nm) of MEA NPs[10,11,14]. These problems limit the compositional space for catalyst research. Recently, 15-element alloy NPs composed of various d-block elements were synthesized on a conductive carbon support with flash heating and cooling by electrically triggered Joule heating with specialized equipment[15]; however, the particle size was approximately 10 nm, and the size distribution was inhomogeneous. For catalytic applications, a general synthesis methodology for smaller ultra-multielement alloy (UMEA) NPs composed of a vast range of elements on the periodic table is highly needed to identify unexplored catalysts.

A liquid-phase chemical reduction method is widely used to synthesize alloy NPs[16,17], and it is known that particle size can be easily tuned by changing the reducing power of the reductant[18]. This method has the potential to be an effective general method to synthesize smaller UMEA NPs. However, most MEA NPs synthesized by chemical reduction methods are composed of elements with high and similar redox potentials, such as platinum-group metals (PGMs)[19,20], and UMEA NPs with more than 10 elements have not yet been reported. This is mainly because of the largely different redox potentials of

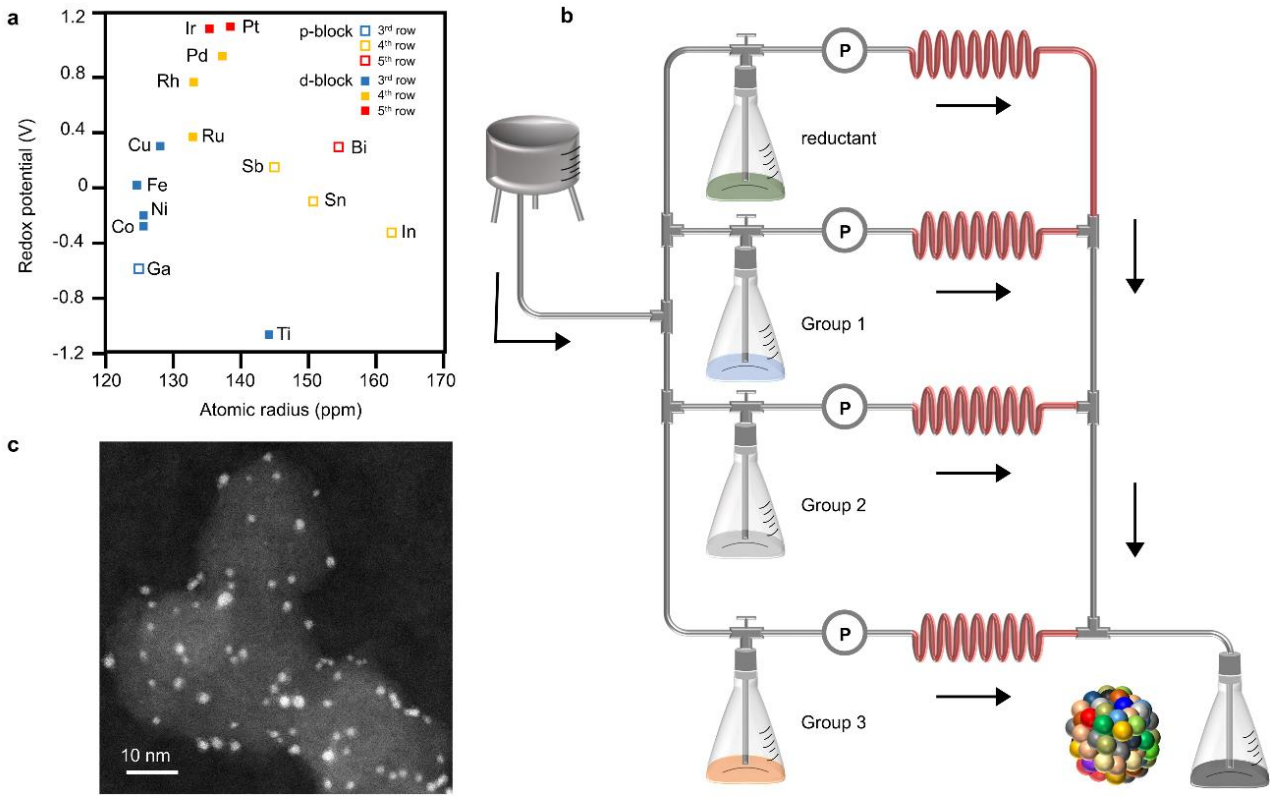

Figure 1. The elements in **15-UMEA** and the developed 4-way flow reactor. **(a)** Redox potentials (V vs. SHE) of the cations in their valence states (Ti^{4+}, Fe^{3+}, Co^{2+}, Ni^{2+}, Cu^{2+}, Ga^{3+}, Ru^{3+}, Rh^{3+}, Pd^{2+}, In^{3+}, Sn^{2+}, Sb^{3+}, Ir^{3+}, Pt^{2+}, Bi^{3+}) and atomic radii (ppm) of the fifteen elements in **15-UMEA**. **(b)** Schematic of the 4-way flow reactor with sequential injections of the metal precursors. Heated areas are coloured red. **(c)** HADDF-STEM image of **15-UMEA**.

multiple elements. To mix a wide variety of elements homogeneously in a nanosized particle,a reductant needs to maintain enough activity to steadily reduce multielement cations concurrently until the reaction is completed. In addition, multielement cations are difficult to treat in the same flask without them undergoing redox reactions with each other. Continuous-flow synthesis can homogenous smaller NPs by precisely controlled stable reaction conditions[21]. Recently, very small and homogeneous IrPdPtRhRu MEA NPs were synthesized with a continuous-flow reactor by injecting all metal precursors simultaenously[22]. Flow chemistry can allow a reductant to maintain enough activity to constantly reduce multielement cations simultaneously until the junction of precursor and reductant solutions. Furthermore, multielement cations can be easily treated in different solutions and mixed under precise control by designing a flow pathway. Therefore, smaller UMEA NPs would be synthesized by flow chemistry with an adequate reducing agent to concurrently reduce a variety of cations via a flow pathway that handles multiple solutions.

In this study, we successfully synthesized ultrasmall BiCoCuFeGaInIrNiPdPtRhRuSbSnTi 15-element UMEA NPs (**15-UMEA**) with a benchtop 4-way continuous-flow reactor to sequentially inject three different solutions of metal precursors by a liquid-reducing method with the strong reducing agent lithium naphthalenide (LiNaph). **15-UMEA** is composed of a wide range of elements from group IV of the early transition metal (Ti) to group XV of the p-block metal (Bi), where the difference between the maximum and minimum redox potentials is over 2 V. **15-UMEA** was characterized by scanning transmission electron microscopy with energy-dispersive X-ray spectroscopy (STEM-EDX), X-ray fluorescence (XRF), hard X-ray photoelectron spectroscopy (HAXPES), powder X-ray diffraction (PXRD), and pair distribution function (PDF) analyses. The STEM-EDX map and point analyses revealed the successful mixing of all 15 elements in a sub-2 nm particle. The amorphous-like structure with short-range order of metal–metal bonds was revealed by PXRD and PDF analysis. We further investigated the electrochemical catalytic properties of **15-UMEA** for alcohol oxidation reactions (AORs) (alcohol: ethanol (EtOR), 1-propanol (PrOR), 1-butanol (BuOR)) in 1 M KOH aqueous solution. We revealed that **15-UMEA** has high durability and high activity for AORs. In addition, **15-UMEA** shows incredibly high forwards-to-backwards current ratios (i_f/i_b) of more than 7 in all AORs, indicating that it promotes complete oxidation reactions and has a high tolerance to CO poisoning[23,24]. These results suggest that the multiple interactions of ultra-multielements efficiently promote multistep complete AORs.

RESULTS AND DISCUSSION

Synthesis and general characterization. As shown in Figure 1a, in the 15 elements (Bi, Co, Cu, Fe, Ga, In, Ir, Ni, Pd, Pt, Rh, Ru, Sb, Sn, and Ti), the atomic radii and redox potentials are very different. The atomic radii of indium (163 ppm) and iron (124 ppm) differ by as much as 31%. It is known that an alloy containing the elements with such a huge atomic radii

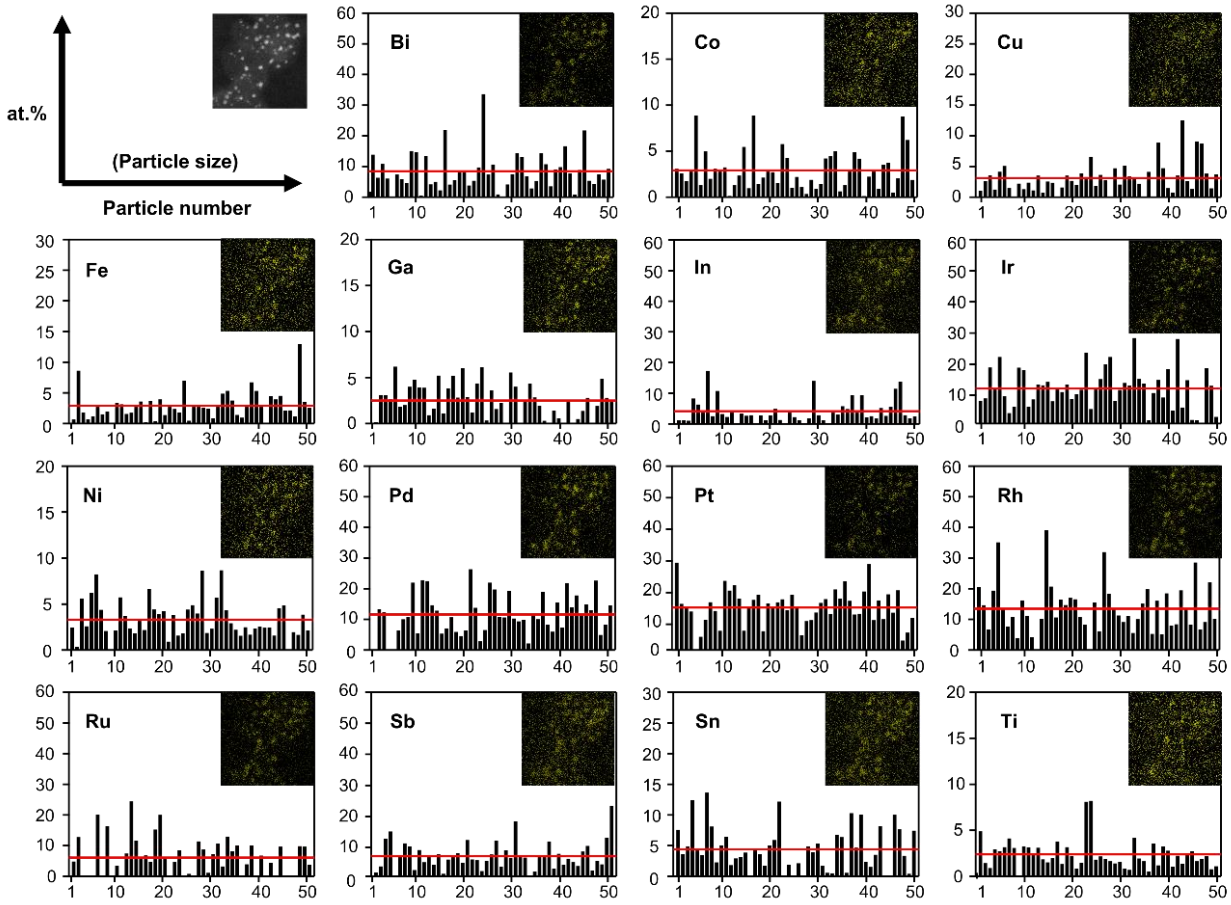

Figure 2. Distribution of the fifteen elements in a particle. Atomic percentages in **15-UMEA** estimated by STEM-EDX point analysis (Bi-L, Co-K, Cu-K, Fe-K, Ga-K, In-L, Ir-L, Ni-K, Pd-L, Pt-L, Rh-L, Ru-L, Sb-L, Sn-L, and Ti-K). The horizontal axis is the particle number in order of increasing particle size (Figure S3). The red lines are the average atomic percentages of fifty particles. Insets: HAADF-STEM image of **15-UMEA** and corresponding EDX maps of each element in **15-UMEA**.

difference tends not to form a solid solution[25]. There is also a large redox potential difference, more than 2 V, between Pt^{2+} (1.2 V vs. SHE) and Ti^{4+} (-1.1 V vs. SHE) (Figure 1a). In addition, some combinations of the precursors may lead to redox reactions such as $2Co^{2+} + Pd^{2+} = 2Co^{3+} + Pd^{0}$. To overcome these problems and synthesize UMEA NPs, the flow path was arranged in a 4-way manner with sequential injections of metal precursors (Figure 1b). In this flow system, the metal precursors were divided into three groups, Group 1 (Co, Fe, Ti), Group 2 (Bi, Ga, In, Ni, Sb, Sn), and Group 3 (Cu, Ir, Pd, Pt, Rh, Ru), based on their redox potential, ligands, and reactivity. These three groups were separately dissolved in tetrahydrofuran (THF), and their solutions were stored in flasks connected to the flow reactor. The solutions of Groups 1 to 3 were injected into the reductant in the order of reduction speed from slower to faster for the simultaneous reduction of multielement cations (Figure 1b). After the reaction, at the exit end of the flow reactor, the solution was mixed with a carbon dispersed solution to load NPs on the carbon support for electrochemical measurements. Although most of the syntheses for MEA NPs were conducted at very high temperatures (~1700 °C), this reaction was performed below the very low boiling point of THF (~66 °C). The high-angle annular dark-field STEM (HAADF-STEM) images (Figures 1c and S1) revealed that the obtained NPs were homogeneously dispersed on carbon and had a 1.9 ± 0.6 nm ultrasmall average particle size. This ultrasmall size and narrow distribution were realized by a strong reducing agent and low synthesis temperature. Assuming a close-packed structure with an average atomic radius of **15-UMEA**, a 1.9 nm particle consists of only 250 atoms at most and has a surface-to-volume ratio of more than 50%, which is expected to be advantageous for catalytic applications.

The composition of **15-UMEA** was characterized by XRF Figure S2), showing that the whole composition of **15-UMEA** was 50% PGMs and 50% the other metals, corresponding to the nominal ratio. To identify the structure of **15-UMEA**, we conducted STEM-EDX map and point analyses. As shown in Figure 2, the EDX maps suggest that all 15 elements are distributed in each NP. However, given that 1.9 nm NPs consist of only 250 atoms, the number of atoms of each element in one particle is expected to be from several to thirty. Hence, to verify the formation of a solid solution in **15-UMEA**, we performed EDX point analysis for 50 randomly chosen particles (Figures 2 and S3) because misidentification of the alloy structure can occur by EDX maps alone. Overall, all 15 elements were observed from most of the single NPs by point analysis. Figure S4 shows the number of constituent elements in 80% of particles is 14 or 15 elements. In most of the particles, all element ratios are below 20%. The red lines show the average atomic ratios of 50 particles, and they are consistent with the XRF results. Although some deviations from the averages are observed in all 15 elements, the deviations are mostly within ±10%,

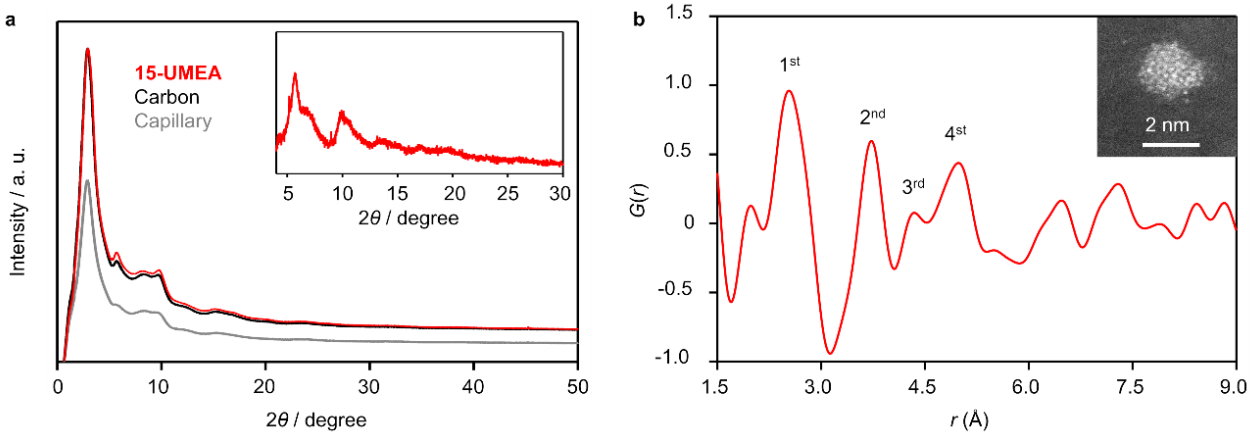

Figure 3. Short-range order in noncrystalline **15-UMEA**. **(a)** Synchrotron XRD patterns of **15-UMEA** (red), carbon (black), and capillary (grey) data. The radiation wavelength was 0.206898(5) Å. Inset: Background-subtracted diffraction pattern of **15-UMEA** (red). **(b)** PDF data of **15-UMEA**. Inset: Atomic resolution HAADF-STEM image of **15-UMEA**.

corresponding to approximately only 25 atoms, which is acceptable as the natural distribution in ultrasmall-sized NPs. In alloy nanoparticles, if all elements are not well mixed and a solid solution is not homogeneously formed, the size dependence of composition should be observed, however, it was not observed in all 15 elements, which also supports the homogeneous distribution of the 15 elements in **15-UMEA** by forming a solid-solution phase. Additionally, all the particles have much higher configurational entropy than the definition of HEA NPs (1.5R, where R is the gas constant)[26], suggesting UMEA formation in all particles (Figure S5).

As a control experiment, we synthesized the same 15-element NPs using a 2-way type flow reactor by injecting all metal precursors dissolved in one solution (Figure S6). In the HAADF image of the 2-way type 15-element NPs Figure S7), the size distribution was larger than that of **15-UMEA** synthesized by the 4-way type reactor, and there were some large NPs of approximately 10 nm in size that were not observed in **15-UMEA**. Figure S8 shows an example of the STEM-EDX point and line analysis results of a large NP. It is revealed that only a few elements, such as In and Pd, are the main constituents and form a core-shell structure. These results strongly suggest that multiway flow synthesis can be a prime candidate for UMEA NPs synthesis because it successfully avoids redox reactions between precursors and achieves the simultaneous reduction of all constituent cations.

Figure 3a shows the PXRD patterns of **15-UMEA**. All the peaks from **15-UMEA** are very weak and broad, and they are not clearly observed. The inset shows the XRD patterns of **15-UMEA** where carbon and capillary patterns were subtracted. In addition, three basic metal structures of fcc, bcc, and hcp are shown in Figure S9. Compared with these patterns, although it is not completely matched with any patterns in the three basic metal structures, the fcc pattern is most similar to the pattern of **15-UMEA**. However, because the XRD pattern of **15-UMEA** cannot be fit by a fcc component, it is concluded that **15-UMEA** has an amorphous-like metal structure with a local order due to a mismatch between the 15-element atomic size and the ultrasmall particle size. This amorphous-like structure was further confirmed by PDF analysis (Figure 3b). The small peak at 1.9 Å corresponds to metal-oxide bonds from surface oxidation due to the ultrasmall size of **15-UMEA** and the absence of an additional protecting agent. The strong peak at approximately 2.6 Å corresponds to various lengths of metal-metal bonds in **15-UMEA**. Assuming a fcc structure with a 2.6 Å nearest bond length, large mismatches from the third nearest distance were found (Figure S10). The inset of Figure 3b is an example of an atomic-resolution HAADF-STEM image of **15-UMEA**. The ordered structure was rarely observed throughout a particle, while a monometallic particle generally has the structure. These results show that **15-UMEA** has a metallic amorphous-like structure with only short-range order. In addition, the particle size can be slightly changed by synthesis temperature (Figure S11).

AORs activity and stability. In MEA NPs, multiple interactions of multiple elements exist, which provides diverse local electronic structures for the surface atoms of MEA NPs[9]. This diverse electronic structure can provide a variety of adsorption/desorption sites that effectively work for different intermediates and substrates in multistep reactions[19]. It is assumed that MEA can catalyse multistep reactions. In addition, multi-element alloys could have high stability in corrosive environments. As a typical example of multistep reactions, we focused on AORs with alkali conditions, which attract attention as key reactions in direct-alcohol fuel cells due to the high energy density of alcohol[27–29]. As control experiments, we synthesized IrPdPtRhRu PGMs 5-element MEA NPs (**5-MEA**)[22], BiCoCuFeGaInNiSbSnTi 10-element MEA NPs (**10-MEA**) which consist of non-PGMs among 15-elements, and Pt and Pd monometallic catalysts loaded on carbon (for details, experimental part in Supporting Information and Figures S12–17). A 1 M KOH with 0.5 M alcohol solution was used for all the measurements. Although Pd or Pt monometallic catalysts are known to have high catalytic activity for AORs, the main problems associated with these catalysts are the surface poisoning effect because the intermediate products of CO_{ad} result in less durability and loss of energy density because the incomplete oxidation reaction transfers only 4 electrons: $C_nH_{2n+1}OH + 5OH^- = C_{n-1}H_{2n-1}COO^- + 4H_2O + 4e^-$ (n: number of carbon in alcohol)[30,31].

Cyclic voltammetry (CV) curves with 50 mV/s of **15-UMEA** showed much higher activity than those of **5-MEA**, **10-MEA**, Pt, and Pd in all AORs (Figures 4a–c and S18). As shown in Figure 4d, interestingly, as the number of carbons increased from ethanol to butanol, the maximum current density of **15-UMEA** also increased; however, the others did not show this

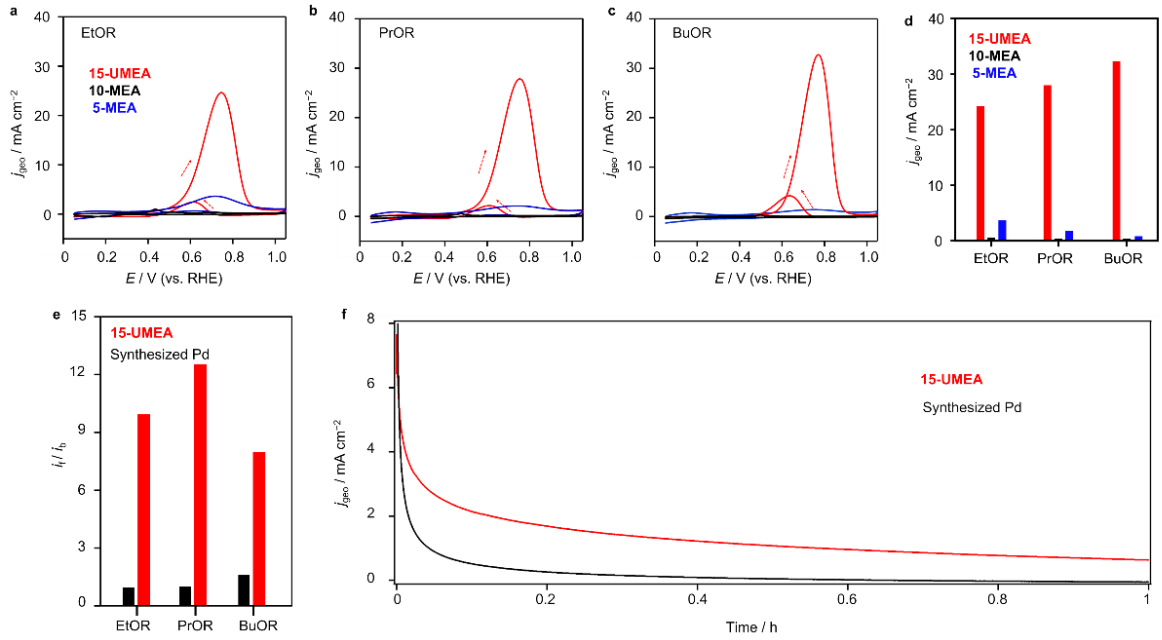

Figure 4. AOR performance of **15-UMEA** in 1 M KOH. **(a)**–**(c)** CVs of **15-UMEA** (red), **10-MEA** (black), and **5-MEA** (blue) in 0.5 M **(a)** ethanol, **(b)** propanol, and **(c)** butanol solutions. **(d)** The maximum current density of **15-UMEA** (red), **10-MEA** (black), and **5-MEA** (blue) in ethanol, propanol, and butanol solutions, respectively. **(e)** i_f/i_b ratios of **15-UMEA** and synthesized Pd in ethanol, propanol, and butanol solutions, respectively. **(f)** Chronoamperometry of **15-UMEA** (red) and synthesized Pd (black) at 0.7 V for 1 hour.

tendency. In addition, **15-UMEA** has 25 times and 88 times larger maximum current density than **5-MEA** and **10-MEA** in BuOR, which implies that **15-UMEA** efficiently promotes the complete oxidation reaction with 6n electrons, including C–C cleavage: $C_nH_{2n+1}OH + 6nOH^- = nCO_2 + (4n + 1)H_2O + 6ne^-$, rather than a partial oxidation reaction with 4 electrons: $C_nH_{2n+1}OH + 5OH^- = C_{n-1}H_{2n-1}COO^- + 4H_2O + 4e^-$. The mass activities are shown in Figure S19. The ratio of forwards current (i_f) to backwards current (i_b) is used for the evaluation of alcohol oxidation completeness and poisoning tolerance for CO_{ad}[23,24]. The catalysts, which have a high i_f/i_b ratio, can efficiently promote the further oxidation of CO_{ad} intermediates during the forwards scan, which means promoting a complete oxidation reaction. For ethanol, propanol, and butanol, **15-UMEA** has a more than 5 times higher i_f/i_b ratio than Pd, which recorded a markedly high value in previously reported representative catalysts[23] (Figures 4e and S20). In addition, ^{1}H NMR measurement shows that the Faradaic efficiency of acetate for 15-UMEA in EtOH oxidation reaction at 0.6V is lower than that of synthesized Pd, which indirectly supports that 15-UMEA efficiently promotes the complete oxidation reaction (Figure S21).

The durability was examined by a chronoamperometry measurement at 0.7 V. While the current density of synthesized Pd drastically decreased to almost 0 within 1 hour, a higher current density was maintained in **15-UMEA** even after 1 hour (Figure 4f). These results suggest that the high-entropy effect in **15-UMEA** contributes to the high tolerance towards CO poisoning.

Based on previous studies of AORs, other than Pt and Pd, the 15 elements are not known to show good activity towards AORs. However, the formation of a solid solution alloy of 15 elements containing a wide range of elements with completely different properties generates an unconventional catalyst surface where each surface atom has a different local electronic structure, which promotes multielementary steps such as C–C cleavage and OH^- adsorption. For example, the dehydrogenation of the first reaction in C–C cleavage is the most difficult step in complete AORs[31,32]. In addition, OH^- adsorption on the catalyst surface at low voltage can also accelerate dehydrogenation and promote further oxidation of the CO_{ad} intermediate on the adjacent metal sites, resulting in high activity and stability[19,33,34]. Although operand measurements for UMEA NPs can be an effective method to discuss the detailed mechanism of catalytic reaction, it was very hard due to the very low density of each element. However, considering the catalytic performance of **5-MEA** and **10-MEA**, nanoparticle surfaces of **15-UMEA** effectively catalyzing AOR would be random distributions of 15 elements in the UMEA, and p-block and early d-block elements on the surface could be oxidized to some extent during the reaction. **15-UMEA** has a featureless broad valence band structure as directly observed by HAXPES (Figure S22), which suggests that each atom has a different local electronic structure[9]. These diverse local electronic structures can provide a large variety of adsorption sites where various intermediates and substrates can adsorb nearby, which can efficiently promote multistep reactions. In contrast, conventional catalysts in which most of the surface atoms have similar local electronic structures seldom promote these different elementary steps simultaneously. Hence, the interactions of all 15 elements can contribute to the high activity and durability of **15-UMEA** to AORs.

Conclusion

In this paper, we first synthesized sub-2 nm UMEA NPs composed of multielements from a wide range from group IV to group XV by a continuous-flow chemical method. The formation of a solid solution of 15 elements, BiCoCuFeGaInIrNiPdPtRhRuSbSnTi, which have completely different properties, was confirmed. In this method, the redox reactions between precursors were suppressed, and the concurrent reduction of all constituent cations was successfully achieved with a multiway flow methodology with sequential injections of metal precursors with a strong reducing agent. **15-UMEA** has high activity

for AORs in ethanol, propanol, and butanol and efficiently promotes complete alcohol oxidation reactions. It is possible to synthesize a variety of UMEA NPs with other composition by this method, however, some elements such as Li which cannot be reduced by the reductant are not available. This report greatly enhances the knowledge on the material design of nanoalloys and promotes material discovery for catalysis.

ASSOCIATED CONTENT

Experimental details, chemicals, HAADF-STEM images, XRF results, schematic of flow reactor, XRD patterns, PDF data, STEM-EDX results, HAXPES spectra, ^{1}H NMR spectra for all compounds, and results of electrochemical measurements.

AUTHOR INFORMATION

Corresponding Authors

$Kohei Kusada − Division of Chemistry, Graduate School of Science, Kyoto University, Kitashirakawa-Oiwakecho, Sakyo-ku, Kyoto 606-8502, Japan; Present Address: The Hakubi Center for Advanced Research, Kyoto University, Kitashirakawa-Oiwakecho, Sakyo-ku, Kyoto 606−8502, Japan;
Email: kusa-da@kuchem.kyoto-u.ac.jp

$Hiroshi Kitagawa -- Division of Chemistry, Graduate School of Science, Kyoto University, Kitashirakawa-Oiwakecho, Sakyo-ku, Kyoto 606-8502, Japan;
Email: kitagawa@kuchem.kyoto-u.ac.jp

Authors

Hiroki Minamihara − Division of Chemistry, Graduate School of Sci-ence, Kyoto University, Kitashirakawa-Oiwakecho, Sakyo-ku, Kyoto 606-8502, Japan;

Tomokazu Yamamoto − The Ultramicroscopy Research Center, Kyushu University, 744 Motooka, Nishi-ku, Fukuoka 819-0395, Japan;

Yasukazu Murakami − The Ultramicroscopy Research Center, Kyushu University, 744 Motooka, Nishi-ku, Fukuoka 819-0395, Japan;

Syo Matsumura − National Institute of Technology, Kurume College, 1-1-1 Komorino, Kurume-shi, Fukuoka 830-8555, Japan;

Loku S. R. Kumara − Center for Synchrotron Radiation Research, Japan Synchrotron Radiation Research Institute (JASRI) SPring-8, 1-1-1 Kouto, Sayo-cho, Sayo-gun, Hyogo 679-5198, Japan;

Osami Sakata − Division of Chemistry, Graduate School of Science, Kyoto University, Kitashirakawa-Oiwakecho, Sakyo-ku, Kyoto 606-8502, Japan;

Shogo Kawaguchi − Center for Synchrotron Radiation Research, Japan Synchrotron Radiation Research Institute (JASRI) SPring-8, 1-1-1 Kouto, Sayo-cho, Sayo-gun, Hyogo 679-5198, Japan;

Yoshiki Kubota − Department of Physics, Graduate School of Science, Osaka Metropolitan University, 1-1 Gakuen-cho, Naka-ku, Sakai, Osaka 599-8531, Japan;

Okkyun Seo − Center for Synchrotron Radiation Research, Japan Synchrotron Radiation Research Institute (JASRI) SPring-8, 1-1-1 Kouto, Sayo-cho, Sayo-gun, Hyogo 679-5198, Japan;

Satoshi Yasuno − Center for Synchrotron Radiation Research, Japan Synchrotron Radiation Research Institute (JASRI) SPring-8, 1-1-1 Kouto, Sayo-cho, Sayo-gun, Hyogo 679-5198, Japan;

Author Contributions

H. M., K. K., and H. K. conceived the idea and designed the research. H. M. performed the synthesis, general characterization, and electrochemical tests. H. M., K. K., T. Y., T. T., Y. M., and S. M. conducted the HAADF-STEM measurements and data analyses. H. M., S. K., O. S., and Y. K. contributed to the synchrotron XRD measurements. L. K. participated in the PDF analysis. O. S., O. S., and S. Y. performed the HAXPES measurements. H. M., K. K., and H. K. discussed the results and wrote the paper. All of the authors discussed and commented on the paper. $K. K. and H. K. contributed equally to this paper.

Notes

Any additional relevant notes should be placed here.

ACKNOWLEDGMENT

We acknowledge the support from a Grant-in-Aid for Specially Promoted Research, No. 20H05623 and Grant-in-Aid for Scientific Research (B), No. 21H01762, and JST PRESTO JPMJPR20A3. This work was partially supported by the Demonstration Project of Innovative Catalyst Technology for Decarbonization through Regional Resource Recycling, the Ministry of the Environment, Government of Japan. Synchrotron XRD measurements were carried out on beamline BL02B2 and BL13XU at SPring-8 under proposal Nos. 2022A1373 and 2022B0598. HAXPES measurements were carried out on beamline BL46XU under proposal Nos. 2022A1394. STEM analyses were supported by "Advanced Research Infrastructure for Materials and Nanotechnology in Japan (ARIM)" of the Ministry of Education, Culture, Sports, Science and Technology (MEXT). Proposal Number JPMXP12222KU0001, and JPMXP12222KU0002.

REFERENCES

(1) Ryoo, R.; Kim, J.; Jo, C.; Han, S. W.; Kim, J. C.; Park, H.; Han, J.; Shin, H. S.; Shin, J. W. Rare-Earth–Platinum Alloy Nanoparticles in Mesoporous Zeolite for Catalysis. *Nature* **2020**, *585* (7824), 221–224. https://doi.org/10.1038/s41586-020-2671-4.

(2) Lv, H.; Lin, L.; Zhang, X.; Li, R.; Song, Y.; Matsumoto, H.; Ta, N.; Zeng, C.; Fu, Q.; Wang, G.; Bao, X. Promoting Exsolution of RuFe Alloy Nanoparticles on $Sr_2Fe_{1.4}Ru_{0.1}Mo_{0.5}O_{6-\delta}$ via Repeated Redox Manipulations for CO_2 Electrolysis. *Nat. Commun.* **2021**, *12* (1), 5665. https://doi.org/10.1038/s41467-021-26001-8.

(3) Feng, J.; Lv, F.; Zhang, W.; Li, P.; Wang, K.; Yang, C.; Wang, B.; Yang, Y.; Zhou, J.; Lin, F.; Wang, G. C.; Guo, S. Iridium-Based Multimetallic Porous Hollow Nanocrystals for Efficient Overall-Water-Splitting Catalysis. *Adv. Mater.* **2017**, *29* (47), 1–8. https://doi.org/10.1002/adma.201703798.

(4) Kusada, K.; Wu, D.; Kitagawa, H. New Aspects of Platinum Group Metal-Based Solid-Solution Alloy Nanoparticles: Binary to High-Entropy Alloys. *Chem. - A Eur. J.* **2020**, *26* (23), 5105–5130. https://doi.org/10.1002/chem.201903928.

(5) Holewinski, A.; Idrobo, J. C.; Linic, S. High-Performance Ag-Co Alloy Catalysts for Electrochemical Oxygen Reduction. *Nat. Chem.* **2014**, *6* (9), 828–834. https://doi.org/10.1038/nchem.2032.

(6) Kusada, K.; Wu, D.; Nanba, Y.; Koyama, M.; Yamamoto, T.; Tran, X. Q.; Toriyama, T.; Matsumura, S.; Ito, A.; Sato, K.; Nagaoka, K.; Seo, O.; Song, C.; Chen, Y.; Palina, N.; Kumara, L. S. R.; Hiroi, S.; Sakata, O.; Kawaguchi, S.; Kubota, Y.; Kitagawa, H. Highly Stable and Active Solid-Solution-Alloy Three-Way Catalyst by Utilizing Configurational-

Entropy Effect. *Adv. Mater.* **2021**, *33* (16), 1–7. https://doi.org/10.1002/adma.202005206.

(7) Zhan, C.; Xu, Y.; Bu, L.; Zhu, H.; Feng, Y.; Yang, T.; Zhang, Y.; Yang, Z.; Huang, B.; Shao, Q.; Huang, X. Subnanometer High-Entropy Alloy Nanowires Enable Remarkable Hydrogen Oxidation Catalysis. *Nat. Commun.* **2021**, *12* (1), 1–8. https://doi.org/10.1038/s41467-021-26425-2.

(8) Mori, K.; Hashimoto, N.; Kamiuchi, N.; Yoshida, H.; Kobayashi, H.; Yamashita, H. Hydrogen Spillover-Driven Synthesis of High-Entropy Alloy Nanoparticles as a Robust Catalyst for CO_2 Hydrogenation. *Nat. Commun.* **2021**, *12* (1), 1–11. https://doi.org/10.1038/s41467-021-24228-z.

(9) Wu, D.; Kusada, K.; Nanba, Y.; Koyama, M.; Yamamoto, T.; Toriyama, T.; Matsumura, S.; Seo, O.; Gueye, I.; Kim, J.; Rosantha Kumara, L. S.; Sakata, O.; Kawaguchi, S.; Kubota, Y.; Kitagawa, H. Noble-Metal High-Entropy-Alloy Nanoparticles: Atomic-Level Insight into the Electronic Structure. *J. Am. Chem. Soc.* **2022**, *144* (8), 3365–3369. https://doi.org/10.1021/jacs.1c13616.

(10) Yao, Y.; Huang, Z.; Xie, P.; Lacey, S. D.; Jacob, R. J.; Xie, H.; Chen, F.; Nie, A.; Pu, T.; Rehwoldt, M.; Yu, D.; Zachariah, M. R.; Wang, C.; Shahbazian-Yassar, R.; Li, J.; Hu, L. Carbothermal Shock Synthesis of High-Entropy-Alloy Nanoparticles. *Science* **2018,** *359*, 1489–1494.

(11) Gao, S.; Hao, S.; Huang, Z.; Yuan, Y.; Han, S.; Lei, L.; Zhang, X.; Shahbazian-Yassar, R.; Lu, J. Synthesis of High-Entropy Alloy Nanoparticles on Supports by the Fast Moving Bed Pyrolysis. *Nat. Commun.* **2020**, *11* (1), 2016. https://doi.org/10.1038/s41467-020-15934-1.

(12) Kusada, K.; Yamamoto, T.; Toriyama, T.; Matsumura, S.; Sato, K.; Nagaoka, K.; Terada, K.; Ikeda, Y.; Hirai, Y.; Kitagawa, H. Nonequilibrium Flow-Synthesis of Solid-Solution Alloy Nanoparticles: From Immiscible Binary to High-Entropy Alloys. *J. Phys. Chem. C* **2021**, *125* (1), 458–463. https://doi.org/10.1021/acs.jpcc.0c08871.

(13) Tsunoyama, H.; Sakurai, H.; Tsukuda, T. Size Effect on the Catalysis of Gold Clusters Dispersed in Water for Aerobic Oxidation of Alcohol. *Chem. Phys. Lett.* **2006**, *429* (4–6), 528–532. https://doi.org/10.1016/j.cplett.2006.08.066.

(14) Wang, X.; Huang, Z.; Yao, Y.; Qiao, H.; Zhong, G.; Pei, Y.; Zheng, C.; Kline, D.; Xia, Q.; Lin, Z.; Dai, J.; Zachariah, M. R.; Yang, B.; Shahbazian-Yassar, R.; Hu, L. Continuous 2000 K Droplet-to-Particle Synthesis. *Mater. Today* **2020**, *35* (May), 106–114. https://doi.org/10.1016/j.mattod.2019.11.004.

(15) Yao, Y.; Huang, Z.; Hughes, L. A.; Gao, J.; Li, T.; Morris, D.; Zeltmann, S. E.; Savitzky, B. H.; Ophus, C.; Finfrock, Y. Z.; Dong, Q.; Jiao, M.; Mao, Y.; Chi, M.; Zhang, P.; Li, J.; Minor, A. M.; Shahbazian-Yassar, R.; Hu, L. Extreme Mixing in Nanoscale Transition Metal Alloys. *Matter* **2021**, *4* (7), 2340–2353. https://doi.org/10.1016/j.matt.2021.04.014.

(16) Zhang, Q.; Kusada, K.; Kitagawa, H. Phase Control of Noble Monometallic and Alloy Nanomaterials by Chemical Reduction Methods. *Chempluschem* **2021**, *86* (3), 504–519. https://doi.org/10.1002/cplu.202000782.

(17) Wu, J.; Gross, A.; Yang, H. Using Carbon Monoxide as Reducing Agent. *Nano Lett.* **2011**, *11*, 798–802.

(18) Schöttle, C.; Bockstaller, P.; Popescu, R.; Gerthsen, D.; Feldmann, C. Sodium-Naphthalenide-Driven Synthesis of Base-Metal Nanoparticles and Follow-up Reactions. *Angew. Chemie - Int. Ed.* **2015**, *54* (34), 9866–9870. https://doi.org/10.1002/anie.201503269.

(19) Wu, D.; Kusada, K.; Yamamoto, T.; Toriyama, T.; Matsumura, S.; Kawaguchi, S.; Kubota, Y.; Kitagawa, H. Platinum-Group-Metal High-Entropy-Alloy Nanoparticles. *J. Am. Chem. Soc.* **2020**, *142* (32), 13833–13838. https://doi.org/10.1021/jacs.0c04807.

(20) Kusada, K.; Mukoyoshi, M.; Wu, D.; Kitagawa, H. Chemical Synthesis, Characterization, and Properties of Multi-Element Nanoparticles. *Angew. Chemie - Int. Ed.* **2022**, *61* (48), e202209616. https://doi.org/10.1002/anie.202209616.

(21) Kusada, K.; Kitagawa, H. Continuous-Flow Syntheses of Alloy Nanoparticles. *Mater. Horizons* **2022**, *9* (2), 547–558. https://doi.org/10.1039/d1mh01413g.

(22) Minamihara, H.; Kusada, K.; Wu, D.; Yamamoto, T.; Toriyama, T.; Matsumura, S.; Kumara, L. S. R.; Ohara, K.; Sakata, O.; Kawaguchi, S.; Kubota, Y.; Kitagawa, H. Continuous-Flow Reactor Synthesis for Homogeneous 1 Nm-Sized Extremely Small High-Entropy Alloy Nanoparticles. *J. Am. Chem. Soc.* **2022**, *144* (26), 11525–11529. https://doi.org/10.1021/jacs.2c02755.

(23) He, Y.; Yan, D.; Wang, S.; Shi, L.; Zhang, X.; Yan, K.; Luo, H. Topological Type-II Dirac Semimetal and Superconductor $PdTe_2$ for Ethanol Electrooxidation. *Energy Technol.* **2019**, *7* (11), 1–6. https://doi.org/10.1002/ente.201900663.

(24) Maiyalagan, T.; Alaje, T. O.; Scott, K. Highly Stable Pt-Ru Nanoparticles Supported on Three-Dimensional Cubic Ordered Mesoporous Carbon (Pt-Ru/CMK-8) as Promising Electrocatalysts for Methanol Oxidation. *J. Phys. Chem. C* **2012**, *116* (3), 2630–2638. https://doi.org/10.1021/jp210266n.

(25) Troparevsky, M. C.; Morris, J. R.; Daene, M.; Wang, Y.; Lupini, A. R.; Stocks, G. M. Beyond Atomic Sizes and Hume-Rothery Rules: Understanding and Predicting High-Entropy Alloys. *Jom* **2015**, *67* (10), 2350–2363. https://doi.org/10.1007/s11837-015-1594-2.

(26) Yeh, J. W.; Chen, S. K.; Lin, S. J.; Gan, J. Y.; Chin, T. S.; Shun, T. T.; Tsau, C. H.; Chang, S. Y. Nanostructured High-Entropy Alloys with Multiple Principal Elements: Novel Alloy Design Concepts and Outcomes. *Adv. Eng. Mater.* **2004**, *6* (5), 299–303. https://doi.org/10.1002/adem.200300567.

(27) Marinkovic, N. S.; Li, M.; Adzic, R. R. Pt-Based Catalysts for Electrochemical Oxidation of Ethanol. *Topics in Current Chemictry* **2019**, *377*, 11. https://doi.org/10.1007/s41061-019-0236-5.

(28) An, L.; Zhao, T. S.; Li, Y. S. Carbon-Neutral Sustainable Energy Technology: Direct Ethanol Fuel Cells. *Renew. Sustain. Energy Rev.* **2015**, *50*, 1462–1468. https://doi.org/10.1016/j.rser.2015.05.074.

(29) Puthiyapura, V. K.; Brett, D. J. L.; Russell, A. E.; Lin, W. F.; Hardacre, C. Biobutanol as Fuel for Direct Alcohol Fuel Cells-Investigation of Sn-Modified Pt Catalyst for Butanol Electro-Oxidation. *ACS Appl. Mater. Interfaces* **2016**, *8* (20), 12859–12870. https://doi.org/10.1021/acsami.6b02863.

(30) Yang, Y. Y.; Ren, J.; Li, Q. X.; Zhou, Z. Y.; Sun, S. G.; Cai, W. Bin. Electrocatalysis of Ethanol on a Pd Electrode in Alkaline Media: An in Situ Attenuated Total Reflection Surface-Enhanced Infrared Absorption Spectroscopy Study. *ACS Catal.* **2014**, *4* (3), 798–803. https://doi.org/10.1021/cs401198t.

(31) Monyoncho, E. A.; Steinmann, S. N.; Michel, C.; Baranova, E. A.; Woo, T. K.; Sautet, P. Ethanol Electro-Oxidation on Palladium Revisited Using Polarization Modulation Infrared Reflection Absorption Spectroscopy (PM-IRRAS) and Density Functional Theory (DFT): Why Is It Difficult to Break the C-C Bond? *ACS Catal.* **2016**, *6* (8), 4894–4906. https://doi.org/10.1021/acscatal.6b00289.

(32) Fang, X.; Wang, L.; Shen, P. K.; Cui, G.; Bianchini, C. An in Situ Fourier Transform Infrared Spectroelectrochemical Study on Ethanol Electrooxidation on Pd in Alkaline Solution. *J. Power Sources* **2010**, *195* (5), 1375–1378. https://doi.org/10.1016/j.jpowsour.2009.09.025.

(33) Lin, H.; Muzzio, M.; Wei, K.; Zhang, P.; Li, J.; Li, N.; Yin, Z.; Su, D.; Sun, S. PdAu Alloy Nanoparticles for Ethanol Oxidation in Alkaline Conditions: Enhanced Activity and C1 Pathway Selectivity. *ACS Appl. Energy Mater.* **2019**, *2* (12), 8701–8706. https://doi.org/10.1021/acsaem.9b01674.

(34) Liang, Z.; Song, L.; Deng, S.; Zhu, Y.; Stavitski, E.; Adzic, R. R.; Chen, J.; Wang, J. X. Direct 12-Electron Oxidation of Ethanol on a Ternary Au(Core)-PtIr(Shell) Electrocatalyst. *J. Am. Chem. Soc.* **2019**, *141* (24), 9629–9636. https://doi.org/10.1021/jacs.9b03474.

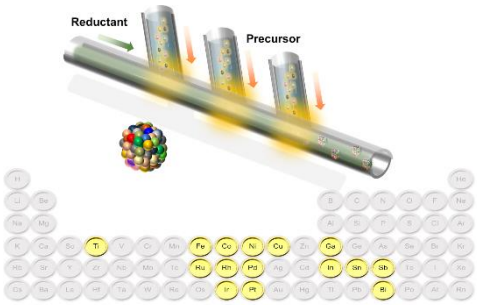
Reductant
Precursor